Dynamic behavior of small-scale model of nailed steep slopes

Debabrata Giri[a]; Aniruddha Sengupta[b]

[a] Institute of Technical Education and Research, Civil Engineering, Bhubaneswar, India [b] Indian Institute of Technology, Kharagpur, Civil Enginnering, Kharagpur, Kharapur, India

First published on: 15 February 2010

PLEASE SCROLL DOWN FOR ARTICLE

Taylor & Francis
Taylor & Francis Group

Dynamic behavior of small-scale model of nailed steep slopes

Debabrata Giri[a,*] and Aniruddha Sengupta[b]

[a]*Institute of Technical Education and Research, Civil Engineering, Jagomora, Jagamahan Nagar, Bhubaneswar, 751030 India;* [b]*Indian Institute of Technology, Kharagpur, Civil Enginnering, Kharagpur, Kharapur, 721302 India*

This paper presents the results of laboratory shaking table tests performed to study the dynamic behavior of reinforced steep slopes. The surface displacements, settlement of the crest and acceleration responses along with strain behavior of the facing wall are examined during the tests. Two 18-cm high steep slopes with slope angles of 60° and 70° are considered. Each slope is reinforced with nine number of hollow aluminum nails placed in three rows. Each nail is glued with three strain gauges to measure the tensile force developed in the nails. Four strain gauges are fixed at the center of the facing wall to measure the development of strains during shaking. The acceleration responses at the base and crest of the model slopes are monitored during the test durations. The numerical simulation of the model tests is performed by a commercial program called FLAC. The numerical results are found to be reasonable close to the corresponding experimental results.

Keywords: shaking table; acceleration response; strain gauge; numerical simulation; FLAC

Notation

c	Cohesion, kPa	ϕ	Angle of friction, degree.
c_c	Coefficient of curvature	$\gamma_{d(max)}$	Maximum dry unit weight, kN/m^3.
c_u	Uniformity coefficient	$\gamma_{d(min)}$	Minimum dry unit weight, kN/m^3.
D_r	Relative density	A	Cross-sectional area of nails, mm^2.
G	Shear modulus, MPa.	ρ	Density of aluminum, kg/m^3.
G_{dyn}	Dynamic shear modulus, MPa.	T_y	Yield strength, N/m^2
K	Bulk modulus, MPa.	T_c	Compressive strength, N
K_{bond}	Shear bond stiffness, kPa.		

1. Introduction

During the 1999 Chi-Chi Earthquake in Taiwan many steep slopes experienced severe damages (Lin *et al.* 2004). Soil nailing technique is one way of protecting slopes especially steep slopes against such catastrophic failure. It provides the soil confinement and stabilizes entire slope. However the seismic resistance and the failure mechanism of nailed soil slope during an earthquake event are not clearly understood and need to be investigated properly. Most of the literature on nailed soil structures emphasizes on the mechanism of reinforcement and the design of structures under static load only. In their studies, Sakaguchi (1996), Koseki *et al.* (1998) and Matsuo *et al.* (1998) have addressed the performance of geosynthetic reinforced retaining walls under seismic condition. The failure mechanisms for slopes under static loading have typically been extended to stability analysis of slopes under seismic loading using pseudo-static approach (Okabe 1924, Mononobe and Matsuo 1997), but the effect of seismic excitation on the failure pattern of slopes are not addressed. Bathurst and Alfaro (1997) also provided extensive reviews of seismic design and performance of geosynthetic reinforced walls, slopes and embankments. However, very few studies on the earthquake resistance and corresponding failure mechanisms of steep nailed slopes are available. Model tests in the laboratory shaking table can shed some lights on the performance of nailed soil structures under dynamic loading condition. With this objective in mind, a shaking table facility has been developed at IIT, Kharagpur to study the nailed embankment slopes under cyclic conditions. This paper presents the results of the laboratory shaking table tests performed to study the dynamic behavior of steep soil slopes reinforced with nails. The surface displacements, settlement of the crest, strain behavior of the

---

*Corresponding author. Email: debagiri@rediffmail.com

facing wall and the accelerations at the base and the crest of the slopes are measured during the tests. The tests, being done on small scale nailed embankment models, suffer from some limitations. The dilation of the sandy soil used in the tests is exaggerated and confining stresses around the nails are small as well. These may lead to under-performance of the soil nails in the tests. However, the tests give some indications regarding the performance of nailed embankments during a dynamic loading condition. The laboratory shaking table tests are also simulated numerically using a large strain finite difference program called FLAC (Itasca Consulting Group, Inc. 2005). The results of the numerical analyses are then compared with those obtained from the laboratory shaking table tests.

2. Development of the shaking table setup

A new shaking table experimental setup is developed at the Indian Institute of Technology, Kharagpur by using a 2800-rpm and 7 HP DC motor. A slotted circular mild steel disc of 300 mm diameter and 20 mm thick is bolted to another circular disc of same size (used as a support to the slotted disc). The supported disc is connected to the shaft of motor. A steel crank shaft 500 mm long, 20 mm in diameter is connected to the slotted disc by bolts. The other end of the crank shaft is connected to a reciprocating rod, 500 mm long and 20 mm in diameter. The amplitude of a sinusoidal motion can be varied by changing the position of the crank shaft in the calibrated slot of the disc. The other end of the reciprocating rod is connected to the shaking table's base plate. The reciprocating rod is kept in the horizontal position during the cyclic motion by a bracket support. The speed of the motor can be controlled from a panel board which essentially consists of an electrical variant.

The reinforced soil slope models are built in a $1.0 \times 0.90 \times 0.48$ m (length × width × height) rectangular test box made up of 10-mm thick Perspex glass sheets to enable observation of deformations of the slopes from the sides. The sides of the box are fixed rigidly with steel angles to prevent any movement. The model box is fixed rigidly to the base plate of the shaking table with bolts. This base plate is fitted with very smooth wheels which slide in horizontal direction on two parallel rails. The three sides of the box are covered with 10-mm thick thermocol sheets to minimize the boundary effects. Sand particles are glued to the bottom surface of the model box to generate surface roughness, so that there is no slippage along the bottom surface during shaking. Acceleration responses during shaking are measured using Delta Tron Accelerometers (B & K Type 4507). Two accelerometers are mounted on the base plate of the shake table to measure the horizontal and the vertical vibrations. Another two accelerometers are fixed on the walls of the test box. One accelerometer is placed at the base of the slope and another one is placed at the crest of the model slope. The Bruel & Kjaer (B&K) Pulse 6.1 system (Type 3560c) sound and vibration meter is used for the data acquisitions. A schematic diagram of the experimental setup and the actual test setup are shown in Figure 1.

The newly developed shaking table has a maximum stroke length of 150 mm and a peak frequency of 50 Hz. A system calibration has been done to check the performance of the experimental setup before starting the experimental work. The objective of the calibration is to verify that the amplification produced by the system is negligible. For calibration purpose, two accelerometers are fixed to the model box wall. The layout of the instruments for the calibration purpose is shown in Figure 2(a). The loading sequence used for the system calibration consists of a 10-s of horizontal sinusoidal motions with peak acceleration of 0.1g at 3.85 Hz frequency and is shown in Figure 2(b). Note that the shaking table accelerates from rest to constant amplitude of 0.1g in 3.57 s. After this it is held constant at 0.1g for 10 s. The initial 3.57 s of motion are not shown in the figure. The responses of the accelerometers are also not shown for this initial 3.57 s. All the measurements are shown for the next 10 s of the input motion during which the amplitude of the sinusoidal motion is held constant at 0.1g.

The responses of the two accelerometers fixed to the model box for the corresponding motion are shown in Figure 2(c). It is observed that no significant amplification of the system is registered during the loading and the system appears to behave linearly throughout the loading history. The responses of the accelerometers are found to be sinusoidal with predominant frequency of 3.85 Hz (Figure 2(d)). This corresponds to a payload of 2 kN (weight of the base plate and the empty model box). The vertical vibration of the shaking base plate and the model box is also measured. The vertical component of the response of the test setup is shown in Figure 3. The magnitude of the vertical vibration (0.0075g) of the base plate is very less as compare to the horizontal input motion and can not significantly affect the test results.

Another important aspect is to ensure that the predominant frequency of the input motion is different from the natural frequency of the model to prevent a resonance condition from developing, which may lead to premature failure. The natural frequency of the base plate along with the test container and the soil slope is determined experimentally by subjecting the whole test setup to a motion and then allowed to shake freely until it stops by its own. As may be seen from the Figure 4, the natural frequency of the whole test setup is much higher than the predominant frequency of the system given in Figure 3.

3. Specimen preparation and material properties

The soil used in this study is a local uniform medium sand (Kasai River sand). The grain size distribution of the sand is shown in Figure 5. It is classified as poorly graded sand (SP), according to the Unified Soil Classification System. The specific gravity of the sand is 2.7. The maximum dry unit weight, $\gamma_{d(max)}$, is 16.7 kN/m^3, and the minimum dry unit weight, $\gamma_{d(min)}$, is 14.03 kN/m^3. The uniformity coefficient (c_u) and coefficient of curvature (c_c) of the sand are found to be 2.84 and 0.87, respectively. In all the model tests, the bulk unit weight of the sand is maintained at 15.02 kN/m^3 and a relative
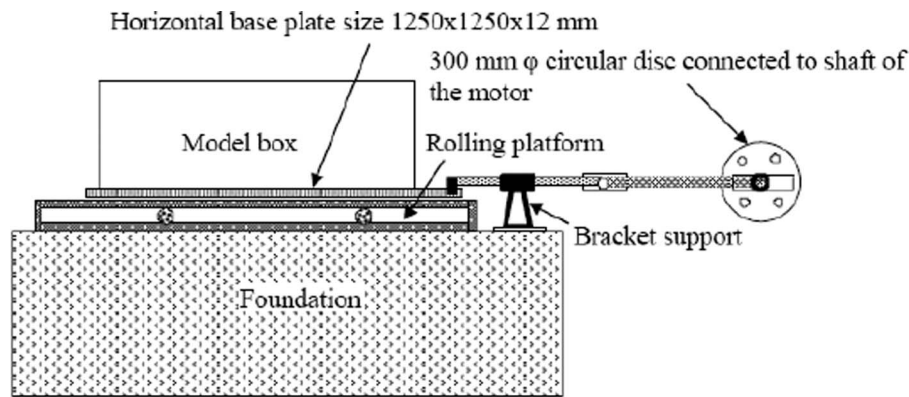
Figure 1.   (a) A schematic diagram of the experimental setup and (b) the actual experimental setup.

density D_r of 60%. The drained triaxial shear test is performed on the soil samples to obtain the shear strength parameters. The cohesion and angle of friction are obtained from triaxial (drained) test as 1.0 kPa and 32°, respectively. Table 1 shows all other soil parameters. Before the construction of the model slopes, 3% water is added to the sand and it is allowed to cure for 24 h in an airtight polythene bag. The model slopes are constructed in the test box by compacting the cured sand up to the desired height by controlled-volume method. The pore water pressure development during cyclic tests and development of suction pressure due to the addition of 3% water to the sand are found to be negligible (Lin *et al.* 2006) for all practical purposes and they do not significantly affect the stability of the slopes tested. Two geo-grid sheets are glued together and kept for more than 48 h and then used as the facing wall. The properties of the facing wall are tabulated in Table 1. During the construction of the model slopes, the facing wall is used to maintain the slope surface at the desired angle.

The performances of two 18-cm high slopes with slope angles of 60° and 70° are studied. In the first stage of the experimental program, the stability of the slopes without any reinforcements is investigated under the cyclic loading condition. In the second phase of the study, the performance of the same slopes reinforced with nails is studied. Each model slope is reinforced with nine numbers of hollow aluminum nails spaced at a constant vertical spacing of 6 cm and a horizontal

spacing of 22 cm. The nails are anchored at right angle to the facing wall. Sand particles are glued to the surface of the nails to generate surface roughness. Three strain gauges of type BKCT-3 (resistance 119.2 ± 0.2 ohms, gauge factor: 1.92± 2% and gauge length 3 mm) are glued at various points of each nail to record local strains. The ratio of length of nail to slope height is maintained at 0.8 for all cases.

4.   Responses of the model slopes

All the model slopes are subjected to the same base acceleration which consists of sinusoidal motions with constant peak amplitude of 0.1g and frequency of 3.85 Hz. This is the same motion for which the test setup is calibrated before. The side view of the failed unreinforced model slopes is presented in Figure 6. It is observed that the unreinforced 70° slope failed at a peak acceleration of 0.08g. The unreinforced 60° slope failed at a peak acceleration of 0.06g. The development of the sliding surface and the crest settlement for the nailed slopes at the end of each test are shown in Figures 7 and 8. The comparison of the behavior of the reinforced and unreinforced slopes in terms of crest settlement at the failure, peak acceleration and number of cycles to failure are given in Table 2. The tests clearly demonstrate how the nail reinforcements have improved the dynamic stability of the steep slopes.

(a)
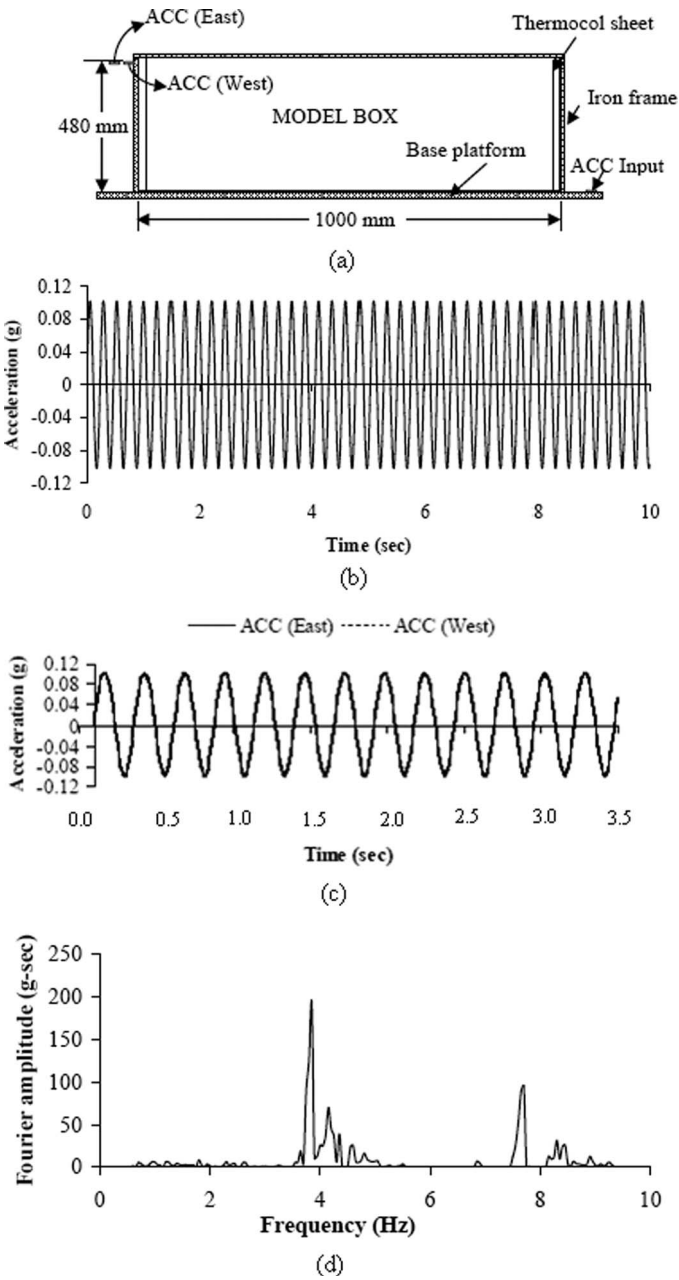

(b)

ACC (East) ······· ACC (West)

(c)

(d)

Figure 2.   (a) Location of the accelerometers in the test setup; (b) input horizontal acceleration; (c) recorded horizontal accelerations in the box during calibration; and (d) frequency content of the measured horizontal acceleration.
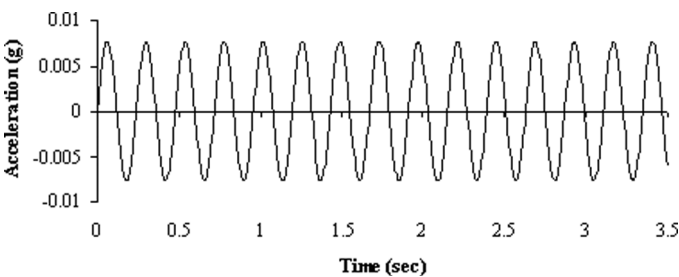

Figure 3.   Measured vertical component of the acceleration during calibration.
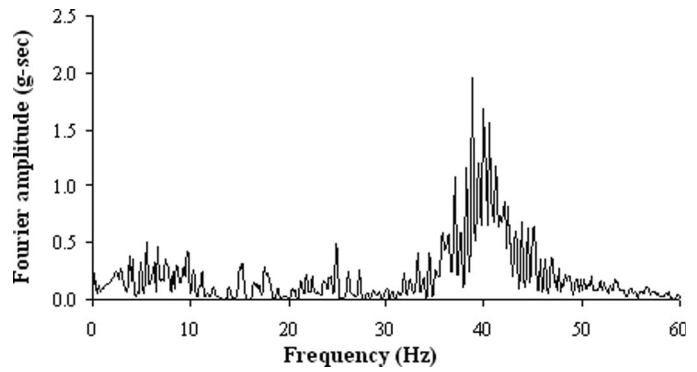

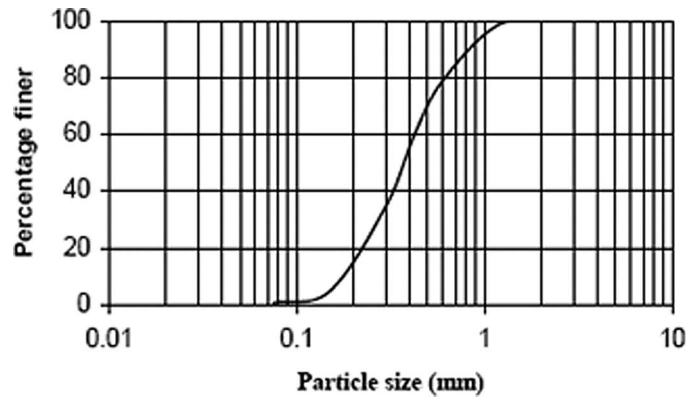Figure 4.   Frequency content of the whole test setup with soil slope.

Figure 5.   Grain size distribution of the Kasai River sand.

The photographs of the failed reinforced slopes are shown in Figures 9 and 10. In all the tests, a gap is developed between the soil slope and the facing wall before the final failure surface is appeared. The magnitude of the gap is found to be more at the crest of the slope. The developed gap at the crest is 102.5 mm for the 60° model slope. In the case of 70° slope, the gap at the crest is found to be 86 mm. The number of loading cycles (only 87) to failure is also less for the 70° model slope as the 60° slope is failed at 117 number of loading cycles. The side views of the failed model slopes show that the facing wall for the 70° model slope has collapsed along with the retaining soil (Figure 10) while for the 60° slope model the facing wall, though separated out from the backfill reinforced soil, is still standing (Figure 9). In both the model slopes, toe failure is observed. The crest settlements are measured at the end of each test when the failure surface has developed completely. The crest settlement for the 70° model slope is 110 mm where as that for the 60° slope it is 102 mm. The area affected during failure is also more for the case of 70° model slope. The top view of the slopes at the end of each test are mapped and shown in Figure 11. The failure surface close to the crest is more or less circular. Some hairline tension cracks at the crest are also prominent. Less number of cracks is developed as the steepness of slope increases. This may be due to the fact that the slope becomes more unstable with the increase in slope angle and the sliding (failure) surface is shallower as the slope fails with less number of loading cycles.

Table 1.   Soil properties of the Kasai River sand

Soil property	Value	Reinforcement property	Value
Unit Weight γ at D_r= 60 %	15.02 kN/m^3	Elastic modulus, E (at 2% strain)	134800GPa
Cohesion, c	1.0 kPa	Yield strength, T_y	5640 N/m^2
Friction Angle, φ	32°	Compressive strength, T_c	0
Static Shear Modulus, G	3.61 MPa	Cross section area, A	201.1428 mm^2
Static Young's Modulus, E	9.528 MPa	Shear bond stiffness, K_{bond}	4.215 MPa
Dynamic Shear modulus, G_{dyn}	23.9 MPa	Density, ρ	2550 kg/m^3
Dynamic Bulk modulus, K_{dyn}	36.3 MPa		
		Facing wall property	*Value*
		Elastic modulus, E (coupon test)	7500.0 MPa
		Tensile Yield Strength	23.45 MPa
		Density	1850.0 kg/m^3

(a) 60^0 slope
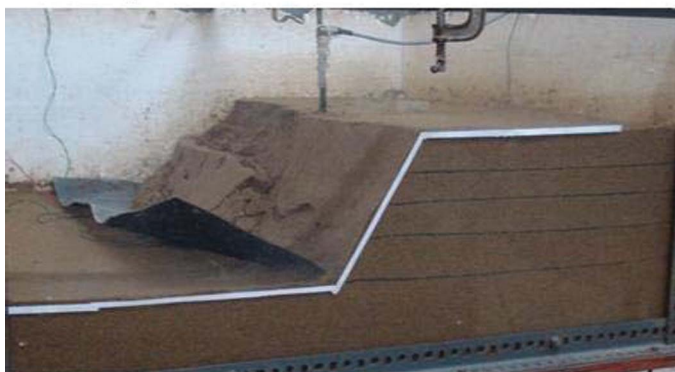
(b) 70^0 slope

Figure 6.   Side views of the failed unreinforced slopes.
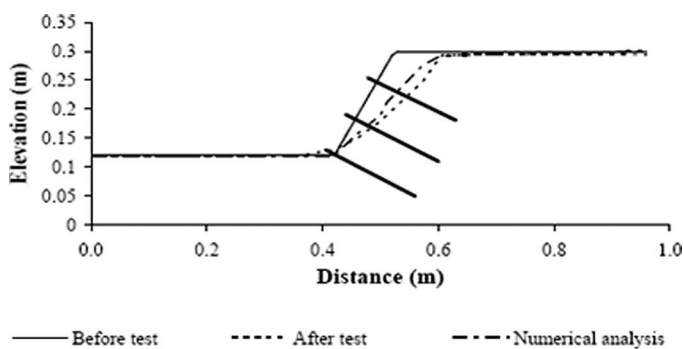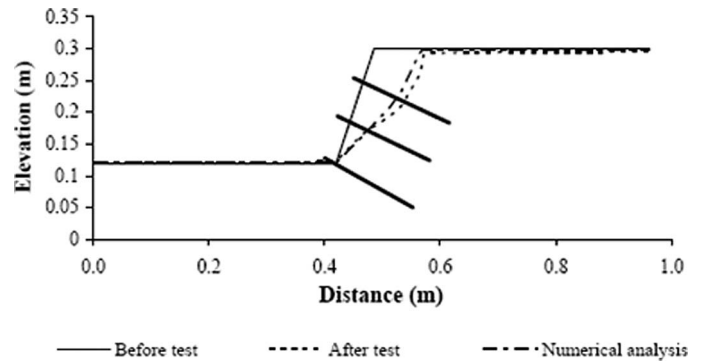

Figure 8.   Comparison of the deformed slopes observed in the experiment and predicted by the numerical analyses for the 70º slope.

Table 2.   Comparison of test results for unreinforced and reinforced slopes

Slope angle (°)	Maximum crest settlement (mm)		Peak acceleration (g)		Number of loading cycles	
	Unreinfoced	Reinforced	Unreinfoced	Reinforced	Unreinfoced	Reinforced
60	56	102	0.08	0.1	43	117
70	68	110	0.06	0.1	32	87

Figure 7.   Comparison of deformed slopes observed in the experiment and predicted by the numerical analyses for the 60º slope.
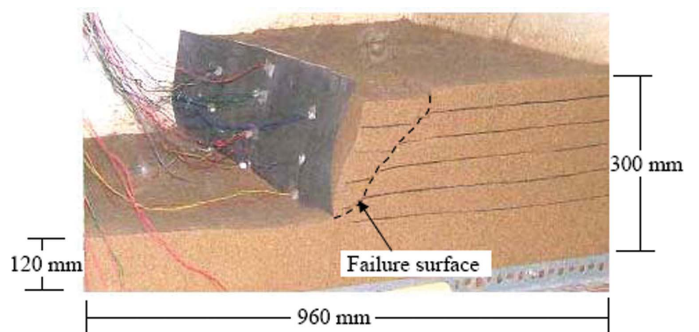

Figure 9.   Side view of the failed 60° slope observed at the end of test.
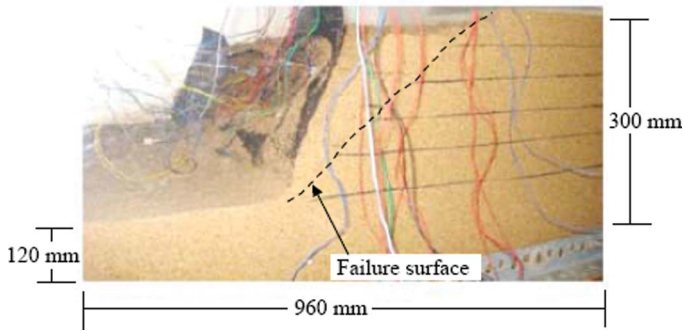
Figure 10. Side view of the failed 70° slope observed at the end of shaking test.
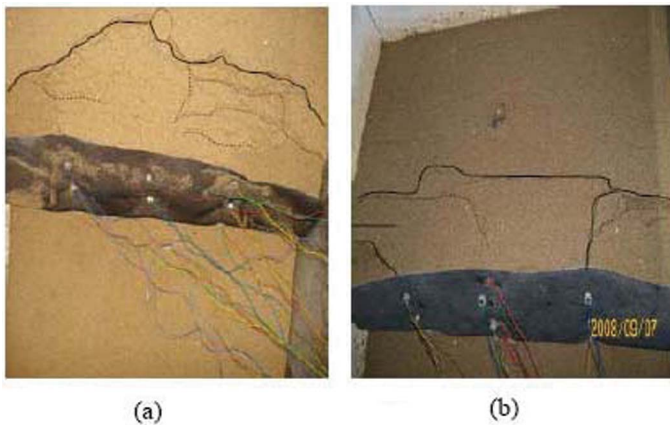

(a)   (b)

Figure 11. (a) Top view of the failed 60° slope at the end of the shaking table tests and (b) top view of the failed 70° slope at the end of test.

Four accelerometers are used to obtain acceleration responses during the tests. The positions of the accelerometers along with the position of nails with strain gauges for a model slope are shown in Figure 12. Two accelerometers are attached to the shaking table base platform to get horizontal and vertical input acceleration parameters, respectively. Another two accelerometers are placed at the centre of the base and the crest of the model slopes to measure amplification of the motion through the slope.

The applied horizontal motions at the base are same for all the cases and also confirmed to be same by the accelerometer located at the base of the slope. The crest acceleration histories of the model slopes are shown in Figures 13 and 14. The amplification of the motion (recorded crest acceleration/input base acceleration) for the model slopes with 60° and 70° slope angles are 1.123 and 1.245, respectively. Table 3 summarizes the magnification of the acceleration through the slopes and the maximum crest settlement recorded in each test.

Local strains corresponding to the loading cycles at different locations of each nail are measured with strain gauges. The reinforcement forces are calculated from the measured average strain using the load versus strain relationship determined from the tensile test on the aluminum nails. The elastic modulus of the aluminum nail is found to be 134.8 GPa in the laboratory by uniaxial tensile test. The variation of reinforcement force as calculated from the strain gauge readings is shown graphically

in Figures 15 and 16. The figures show that the induced nail forces varied nonlinearly with respect to the loading. The induced reinforcement force is more for the steeper slope. The maximum induced force is 269.56 N for the 70° model slope as against 262.2 N for the 60° model slope. As the slope angle increases the mass of the failure wedge increases. This may be season why the induced force is more for the steeper slope. The top most nail does not generate significant force as compare to other nails. This is likely due to the lack of adequate soil confinement at the shallow depth. The maximum axial forces developed at the end of the prescribed motion are also compared with the values obtained by the pseudo-static analysis (Saran 2005) and presented in Table 4.

Four strain gauges are fixed at the mid width of the facing wall to obtain the lateral earth pressure on the wall during the motions. The positions of the strain gauges are 5, 55, 115 and 175 mm, respectively, from the bottom of the model slopes. The average variation of pressure with respect to the slope height is shown in Figure 17. A minimal pressure is obtained at the top of the facing wall. These induced pressures depend on the pseudo-static forces and mass of the failure wedge. The maximum pressure is obtained near about the centroid of the slope.

5. Numerical analysis of the model slopes

The computer program FLAC developed by the Itasca Consulting Group (2005) is utilized for the dynamic analyses of the nine slopes tested in the laboratory shaking table. The FLAC has been successfully used in the past (Roth *et al.* 1993, Wang 2001, Wang *et al.* 2004) for the dynamic analysis of soil embankments. The FLAC (Fast Lagrangian Analysis of Continua) computes stresses and strains in a continuum by a finite difference method. It uses an explicit solution method. The Lagrangian analysis allows for large distortions of the grid so that the end state at each node is the beginning state of the next stress cycle. In the numerical modeling, only the soil slopes are modeled. The container and the shaking table are not modeled. The soil is modeled as a material obeying the Mohr-Coulomb yield criteria. The soil slopes are discretized by quadrilateral elements. The maximum element size is well within 1/12 of the longest wave length. This provides accurate wave transmission within the soil model. A typical discretized soil slope is shown in Figure 18. The bottom of the slopes is assumed to be fixed. The two side boundaries are assumed to be on roller (horizontal deformation is restricted). The nail reinforcements are modeled as cable elements. The bending effects are not important as the cable elements are sufficient to allow the modeling of a shearing resistance along their length. It is provided by the shear resistance (bond) between the cable elements and the soil mass. The cable element formulation in FLAC considers more than just the local effect of the reinforcement. Its effect in resisting deformation is accounted for along its entire length. The cable is assumed to be divided into a number of segments with nodal points located at each end of a segment. The mass of each segment is lumped at the nodal
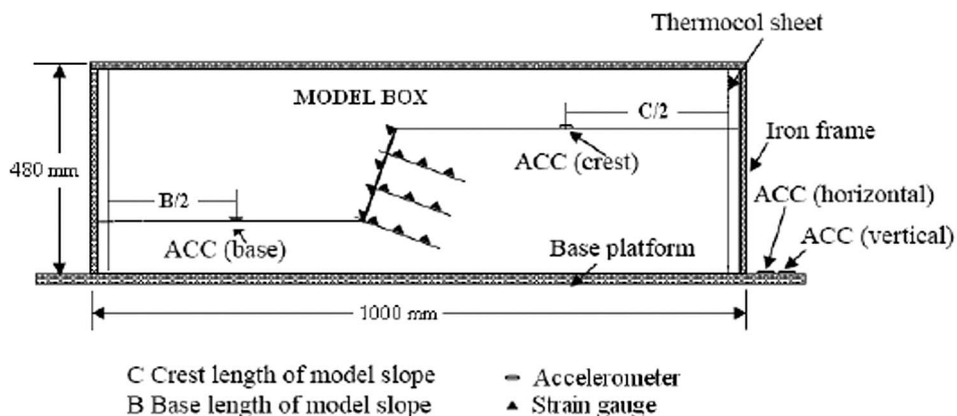
Figure 12. Test setup, location of the accelerometers and location of strain gauges on the nails.
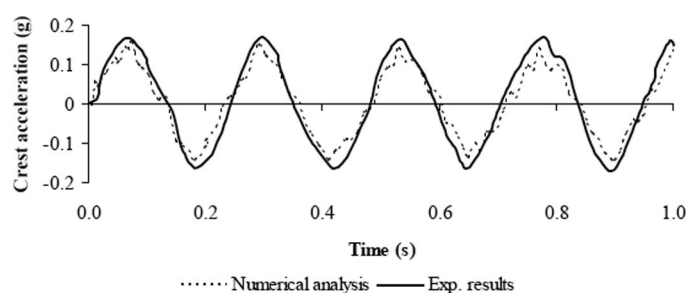

Figure 13. Comparison of crest accelerations in the laboratory experiments and the numerical analyses for the 60° slope.
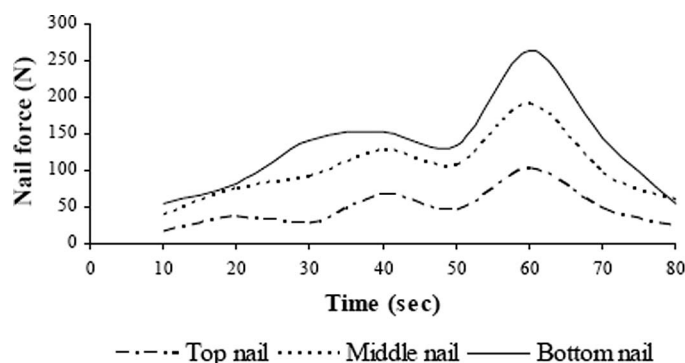

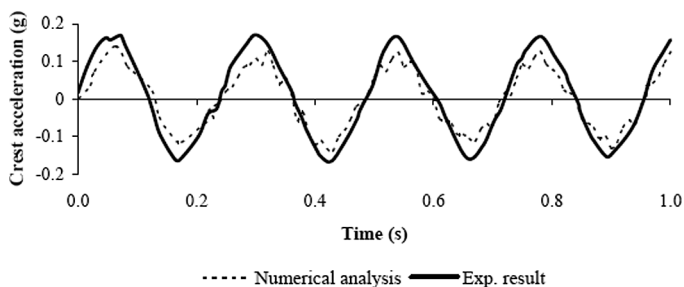Figure 15. Variation of nail force (N) for the 60° slope.

Figure 14. Comparison of crest acceleration in the laboratory experiments and the numerical analyses for the 70° slope.
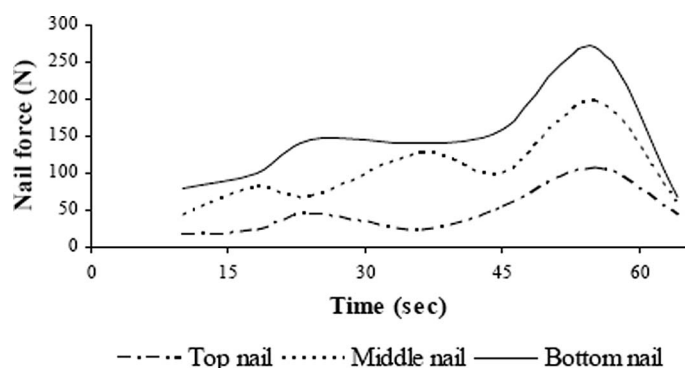

Figure 16. Variation of nail force (N) for the 70° slope.

Table 3. Comparison of the crest settlement and crest acceleration amplification factor

Slope angle (°)	Experimental results		Numerical results	
	Maximum crest settlement (mm)	Amplification at crest	Maximum crest settlement (mm)	Amplification at crest
60	102	1.123	96	1.098
70	110	1.245	103	1.196

Table 4. Comparison of the maximum axial force (N) on nails at end of the test

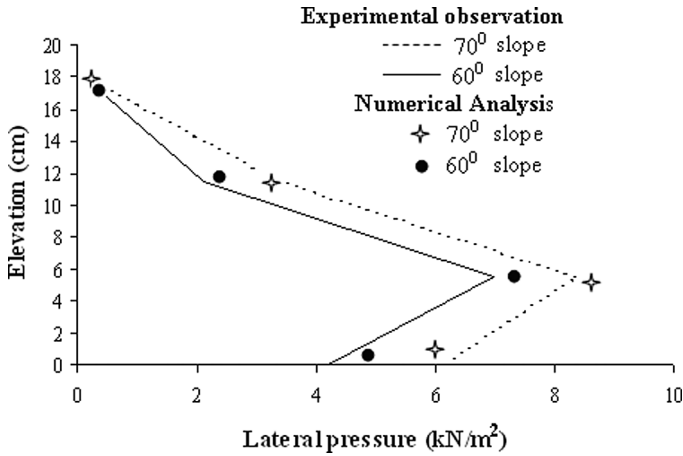| Slope angle (°)	Experimental results			Numerical results			Pseudo-static analysis		
	Top	Middle	Bottom	Top	Middle	Bottom	Top	Middle	Bottom
60	1.5	2.44	2.85	2.41	2.76	3.28	1.78	3.14	3.6
70	1.7	2.95	5.31	1.63	3.23	5.17	1.838	3.44	5.82

Figure 17. Comparison of the variation of lateral pressures against the facing wall.

points, as in the continuum formulation of FLAC. The axial behavior of reinforcement systems is assumed to be governed entirely by the reinforcing element itself. As the reinforcing element is slender, it offers little bending resistance and can be treated as a one dimensional member with capacity to sustain uniaxial tension only. In the present analysis, the axial stiffness is described in terms of nail cross-sectional area and Young's modulus, E. The aluminum nails are installed at a regular spacing of 0.22 m in the horizontal direction. The spacing of nails is used to automatically scale reinforcement properties. The actual cable forces in the cable elements are automatically calculated by the program. The shear bond stiffness K_{bond} for nail can be calculated from a numerical estimate for the elastic shear stress, τ_G, obtained from an equation describing the shear stress at the grout interface (St. John and Van Dillen 1983).

$$\tau_G = \frac{G}{(D/2 + t)\ln(1 + 2t/D)}\nabla u \quad (1)$$

where ∇u is the relative displacement between the element and the surrounding material; G is the grout shear modulus; D is the reinforcement diameter, and t is the annulus thickness. However, FLAC also permits the following expression to provide a reasonable estimate of K_{bond}

$$k_{bond} = \frac{2\pi G}{10 \ln(1 + 2t/D)} \quad (2)$$

The one-tenth factor in the above equation helps to account for the relative shear displacement that occurs between the nail and the actual borehole surface. This relative shear displacement (∇u) is not accounted for in the present formulation. The computed K_{bond} and other material properties of the aluminum nail as obtained from the laboratory tests are tabulated in Table 1. The cohesion, c, friction angle, ϕ, unit weight, γ, dynamic shear modulus, G_{dyn} and dynamic bulk modulus, K_{dyn} are specified for the soil. The soil parameters are based on the laboratory test results and are summarized in Table 1. The facing wall is modeled as a continual liner element (FLAC 2005). In order to analyze the gap developed between the facing wall and the soil slope, an interface element is introduced between them. Numerical analyses show that the gap developed is more near the crest of the model slopes. The magnitude of the gap at the crest of the model slope with 70° and 60° slope angles is found to be 62.15 and 90.5 mm, respectively (Figure 19). This finding is in good agreement with the observed test results. At the beginning, a gravity turn-on analysis is performed and the stresses are allowed to reach equilibrium state in static condition under self weight only.

The dynamic analysis is then followed by prescribing the horizontal acceleration at the base of the model. This acceleration is the same sinusoidal motion recorded by the accelerometers fixed to the shaking table. The wave reflections at the two extreme side boundaries are minimized by specifying free field boundary conditions at those locations. The crest acceleration, and slope deformations are calculated with time. The Figures 8 and 9 show the displacement of the slopes at the end of the shaking and compare them with those observed in the laboratory shaking table tests. Numerical analyses predict a maximum crest settlement of 96 and 103 mm, respectively, for the 60° and 70° model slopes. The amplification factor of the crest acceleration for the 70° and 60° model slopes are 1.196 and 1.098, respectively. These numerical findings are also in good agreement with the laboratory test results. The crest acceleration computed for each case is compared with that recorded in the corresponding shaking table test in Figures 13 and 14. The lateral earth pressures of the backfill against the facing wall during ground motions are also numerically obtained and a comparison with the test results is
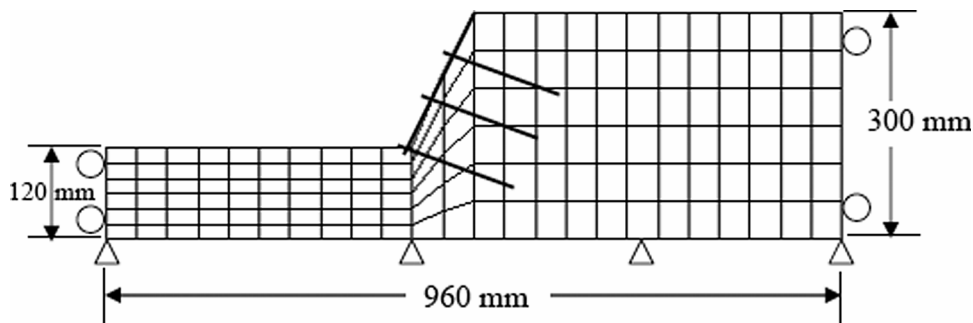

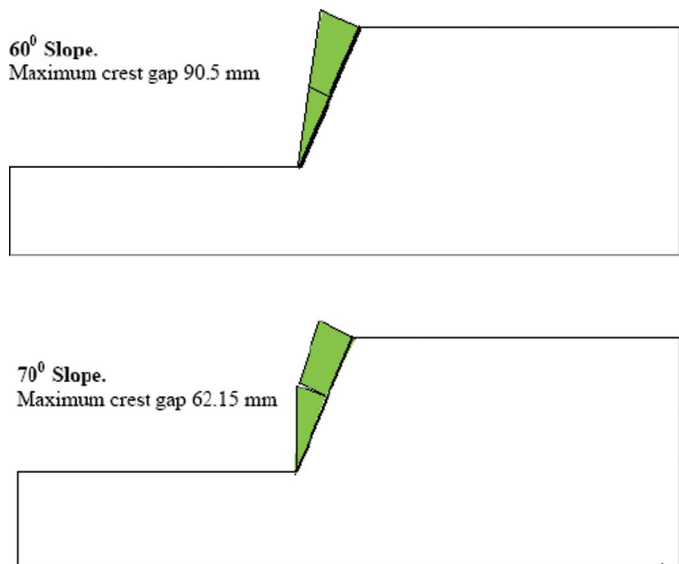Figure 18. Discretization of a typical nailed soil slope.

Figure 19. Developed gap between the backfill and facing wall as obtained in the numerical analysis.

Figure 20. Comparison of the axial nail force (N) along the nails.

shown in Figure 17. The axial forces along each nail are also numerically found and compared with the test results in Figure 20. The displacement vectors at the end of motions along with the theoretical failure surfaces for the model slopes predicted by FLAC are shown in Figure 21. The magnitude of the maximum displacement for the steeper slope is more. The maximum crest settlement and the amplification of motion through
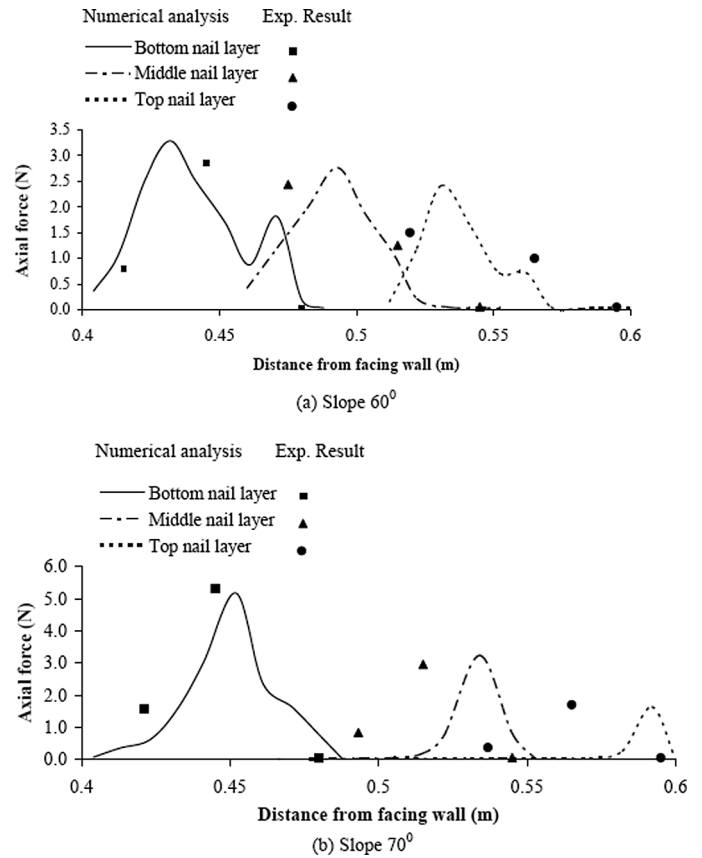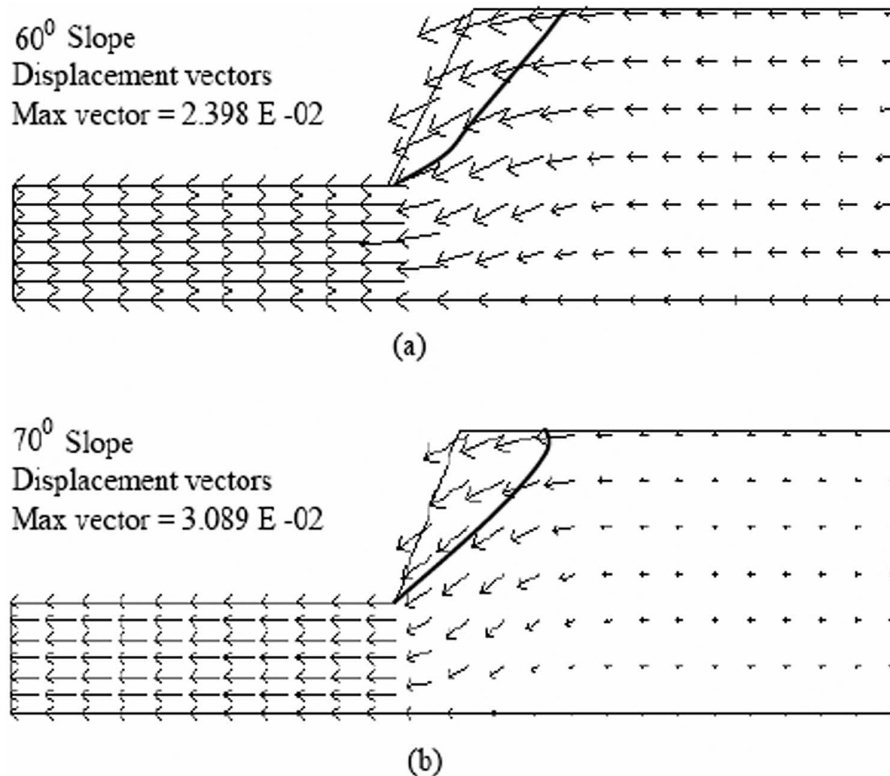

Figure 21. Displacement vectors and the predicted failure surface in the numerical analyses.

the slope are shown and compared with the corresponding test results in Table 3. The numerical results are in reasonable agreements with the laboratory shaking table results.

6. Conclusions

Based on the present study on the dynamic behavior of nailed soil slopes, the following conclusions are drawn:

The failure surfaces appeared to be circular and confined to the zone near the slope surfaces. The observed failure surface is deeper for the steeper slope. The top view of failed slopes shows that numbers of major cracks along with some hairline cracks are developed near the box boundary walls. Some intermediate cracks are also developed near the boundary and between major failure surfaces. It is likely that more than one set of failure surfaces might have developed during the laboratory shaking table tests. Number of cracks appeared to be less as the slope angle increases. With the increase in slope angle, the slope becomes more unstable and fails with less number of loading cycles. The mass movement and size of possible failure wedge decrease with decrease in loading cycles. This may be the reason for the development of less number of failure cracks in the steeper slope. The induced nail force varied nonlinearly with respect to loading cycles and the top nail does not generate significant force as compared to the other nails. This is likely due to the lack of adequate soil confinement. A minimal strain value is obtained at the top of the facing wall. The maximum strain is obtained near about the centroid of the slope. The magnification of the amplitude of the crest acceleration for steeper slope is more. The numerical analyses adequately reproduced the responses of the model slopes in the frequency and the time domains. The slope and crest displacements computed by the FLAC are found to be reasonably close to those observed in the shaking table tests. The gap predicted between the soil slope and the facing wall by the numerical analyses is also found to be comparable with that observed in the laboratory shaking tests.

References

Bathurst, R.J., and Alfaro, M.C. 1997. Review of seismic design, analysis and performance of geosynthetic reinforced walls, slopes and embankments. Invited key note paper. In. Earth Reinforcement: IS: Kyushu 96, Proceedings of the 3rd International Symposium on Earth Reinforcement, Fukuoka, Japan, Balkama Rotterdam, The Netherlands, pp. 887–918.

Itasca Consulting Group, Inc. FLAC Version 5, 2005. Fast Lagrangian Analysis of Continua: Theory & Background. Minneapolis, MN, USA.

Koseki, J., Munaf,Y., Tatsuoka, F., Tateyama, M., Kojima, K., and Sato, T., 1998. Shaking and tilt table tests of geosynthetic reinforced soil and conventional type retaining walls. *Geosynthetic International*, 5 (1–2), 73–96.

Lin, C.W., Shieh, C.L., Yuan, B.D., Shieh, Y.C., Liu, S.H., and Lee, S.Y., 2004. Impact of Chi-Chi earthquake on the occurrence of landslides and debris flows: example from the Chenyulan River watershed, Nantou, Taiwan. *Engineering Geology*, 71 (1–2), 49–61.

Matsuo, O., Tsutsumi, T., Yokoyama, K., and Saito, Y., 1998. Shaking table tests and analyses of geosynthetic-reinforced soil retaining walls. *Geosynthetic International*, 5 (1–2), 97–126.

Mononobe, N., and Matsuo, H., 1997. On the determination of earth pressure during earthquake. *In: Proceeding of the World Engineering Conference*, Tokyo, Japan, p. 176.

Okabe, S., 1924. General theory on earth pressure and seismic stability of retaining wall and dam. *Journal of the Japanese Society of Civil Engineering*, 10 (6), 1277–1324.

Roth, W.H., Inel, S., Davis, C., and Brodt, G., 1993. Upper San Fernando Dam 1971 revisited. *Annual Conference Proceedings of the Association of State Dam Safety Officials*, D.W. Darnton and S.C. Plathby, eds, Lexington, KY, pp. 49–60.

Sakaguchi, M., 1996. A study of the seismic behavior of geosynthetic-reinforced walls in Japan. *Geosynthetic International*, 3 (1), 13–30.

St. John, C.M., and Van Dillen, D.E., 1983. Rock bolts: A new numerical representation and its application in tunnel design in rock mechanics – Theory – Experiment – Practice. *In: Proceedings of the 24th U.S. Symposium on Rock Mechanics*, Texas A &M University, pp. 13–26.

Saran, S., 2005. Reinforced soil and its engineering application. I.K. International Pvt. Ltd. Wang, Z.L., 2001. Simulation of earthquake performance of a waterfront slope using fully coupled effective stress approach. FLAC and numerical modeling in Geomechanics, Proceedings of the 2nd International FLAC Conference, Lyon, France, pp. 101–108.

Wang, Z.L., Makdisi, F.I., and Egan, J., 2004. Practical applications of a nonlinear approach to analysis of earthquake-induced liquefaction and deformation of earth structures. *In: Proceedings of the 11th International Conference on Soil Dynamics & Earthquake Engineering*, University of California, Berkeley, CA, 2, 299–306.